

Showcasing research from Professor Sekine's laboratory,
Department of Applied Chemistry, Waseda University,
Tokyo, Japan.

First observation of surface protonics on SrZrO_3 perovskite
under a H_2 atmosphere

This is the first direct observation that surface proton
hopping occurs on SrZrO_3 perovskite even under a H_2
(i.e. dry) atmosphere.

As featured in:



See Yasushi Sekine *et al.*,
Chem. Commun., 2020, **56**, 2699.



Cite this: *Chem. Commun.*, 2020, 56, 2699

Received 9th November 2019,
Accepted 21st January 2020

DOI: 10.1039/c9cc08757e

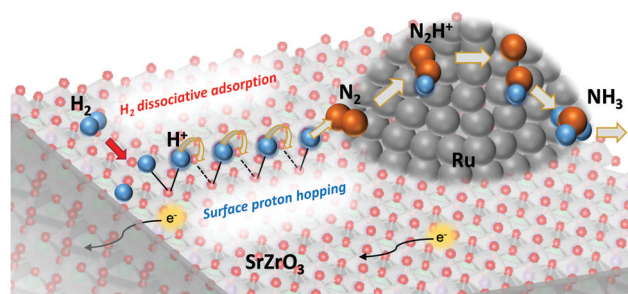
rsc.li/chemcomm

First observation of surface protonics on SrZrO₃ perovskite under a H₂ atmosphere†

Yudai Hisai,^a Kota Murakami,^a Yukiko Kamite,^a Quanbao Ma,^b Einar Vøllestad,^b Ryo Manabe,^a Taku Matsuda,^a Shuhei Ogo,^a Truls Norby^b and Yasushi Sekine^{id} *^a

This is the first direct observation that surface proton hopping occurs on SrZrO₃ perovskite even under a H₂ (*i.e.* dry) atmosphere. Understanding proton conduction mechanisms on ceramic surfaces under a H₂ atmosphere is necessary to investigate the role of proton hopping on the surface of heterogeneous catalysts in an electric field. In this work, surface protonics was investigated using electrochemical impedance spectroscopy (EIS). To extract the surface proton conduction, two pellets of different relative densities were prepared: a porous sample (R.D. = 60%) and a dense sample (R.D. = 90%). Comparison of conductivities with and without H₂ revealed that only the porous sample showed a decrease in the apparent activation energy of conductivity by supplying H₂. H/D isotope exchange tests revealed that the surface proton is the dominant conductive species over the porous sample with H₂ supply. Such identification of a dominant conductive carrier facilitates consideration of the role of surface protonics in chemical reactions.

Surface protonics is recognized as proton transportation on an oxide surface in a middle-temperature or low-temperature region. In a H₂O atmosphere, protons are transferred continuously between M–OH₂⁺ and M–OH[–] formed by supplied H₂O by the Grotthuss mechanism.^{1–3} Investigation of surface protonics is anticipated to yield useful knowledge for application to various electrochemical devices such as fuel cells, chemical sensors, and electrolyzers.^{4–6} Recently, an important role of surface protonics during heterogeneous catalytic reactions was found in an electric field under both H₂O and H₂ atmospheres.^{7–19} It promotes low-temperature catalysis for hydrogen production, ammonia synthesis, and other processes. Electrochemical impedance spectroscopy (EIS) of oxide surfaces under a H₂O atmosphere has been investigated to elucidate the correlation between catalysis in an electric field and surface



Scheme 1 Contribution of surface protonics in the heterogeneous catalytic reaction for low temperature (<550 K) ammonia synthesis in an electric field.¹²

protonics (Scheme 1).^{8,10,20} The results show a good agreement between the H₂O partial pressure dependence on surface protonics and that on catalytic activity in the electric field.²⁰ The correlation revealed the strong contribution of surface protonics to the enhanced reaction rate at a low temperature in the electric field. Therefore, EIS measurement is a promising method for the evaluation of surface protonics during catalytic reaction with an electric field.

This study provides the first example of the observation of surface protonics under a H₂ atmosphere (*i.e.* in a dry condition) using EIS measurements. As the sample, SrZrO₃, which was used for ammonia synthesis in the electric field, was selected. Measurements were performed with porous (relative density, R.D. = 60%) and dense (R.D. = 90%) SrZrO₃ pellets. Earlier reports have described that porous pellets that have low relative density (R.D. = 50–60%) are feasible for extracting surface conductive components^{4,5,20–25} because many more vacant sites exist for adsorbate species to adsorb on the oxide surface than on dense pellets (R.D. > 90%). Surface protonics was confirmed from comparison of the respective behaviors of porous and dense samples.

We prepared two types of SrZrO₃ pellets having low (60%) and high (90%) densities. SrZrO₃ powders were synthesized using a complex polymerization method.^{12,14,16} Then porous and dense SrZrO₃ pellets were prepared. The detailed preparation method

^a Department of Applied Chemistry, Waseda University, 3-4-1 Okubo, Shinjuku, Tokyo, 169-8555, Japan. E-mail: ysekine@waseda.jp

^b Department of Chemistry, University of Oslo, FERMI, Gaustadalléen 21, NO-0349 Oslo, Norway

† Electronic supplementary information (ESI) available: Preparation method for the sample, Fig. S1 and S2. See DOI: 10.1039/c9cc08757e



is described in the ESI.[†] All electrochemical impedance spectroscopy (EIS) measurements were taken in a measurement cell (ProboStat[™], NORECS AS, Norway) using a two-electrode four-wire setup connected to an impedance spectrometer (alpha-A; Novocontrol Technologies) with a ZG4 interface. The impedance spectra were recorded at frequencies of 10^6 – 10^{-3} Hz using an oscillation amplitude of 100 mV RMS (root mean square). Temperature dependences of electrochemical conductivity were examined under a N₂ atmosphere at 423–723 K and under N₂:H₂ = 1:3 at 348–723 K. Impedance data were analyzed using ZView equivalent circuit fitting software (ver. 3.5a; Scribner Associates Inc.) using a [(RC)(RC)]C_{stray} equivalent circuit model, as presented in Fig. S1 (ESI[†]). The (RC) components were assigned to the series-connected bulk and grain boundary transport. Also, C_{stray} denotes parallel-connected parasitic capacitance. The values of electrochemical conductivity (σ) were calculated for both the bulk (b) and grain boundary (gb) using eqn (1). In this equation, L represents the pellet thickness, S denotes the area of the Pt electrode, and R stands for the fitted resistance value. The apparent activation energy (E_a) of the electrochemical conductivity was calculated for both the bulk and grain boundary using the Arrhenius expression. For eqn (2), where A shows the pre-exponential, k_B denotes Boltzmann's constant.

$$\sigma_x = L/SR_x \quad (x = b, gb) \quad (1)$$

$$\sigma_x T = A \exp(-E_a/k_B T) \quad (2)$$

X-ray photoelectron spectroscopy (XPS) measurements (Versa Probe II; Ulvac-Phi Inc.) were carried out with an Al K α X-ray source. The binding energies were calibrated using the C1s peak at 284.8 eV.^{26,27} The pre-treatment conditions were classified into 3 patterns: (A) N₂ purge at 723 K for 2 h, (B) H₂ reduction under a N₂:H₂ = 1:3 atmosphere at 723 K for 2 h, and (C) N₂ purge for 2 h after H₂ reduction at 723 K for 2 h.

The crystalline phases for the synthesized SrZrO₃ powder and pellets were evaluated from XRD measurements. As presented in Fig. S2 (ESI[†]), all samples have an orthorhombic perovskite structure. According to the XRD peak intensity and width, crystallinity increased in the following order: powder < porous pellet < dense pellet. Moreover, the crystal morphologies of both the porous and dense pellets were assessed using FE-SEM, as depicted in Fig. 1. Numerous pores were detected in the porous pellet. Such a porous sample is extremely useful for the detection of surface conduction induced by the adsorbed H₂O on the grain surface at low temperatures under H₂O conditions.^{4,5,20–25}

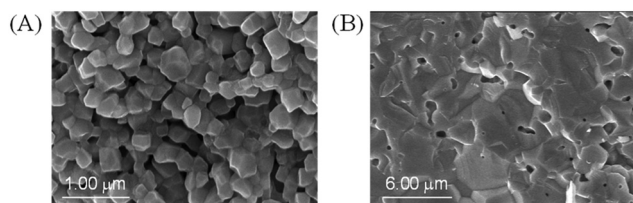


Fig. 1 FE-SEM images of SrZrO₃: (A) porous pellet (R.D. = 60%) and (B) dense pellet (R.D. = 90%).

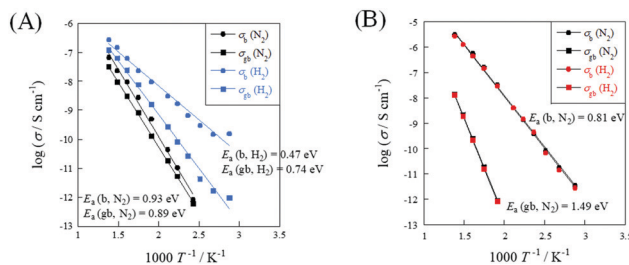


Fig. 2 Temperature dependences of electrochemical conductivity under N₂ and H₂ atmospheres: (A) porous SrZrO₃ pellet (R.D. = 60%); and (B) dense SrZrO₃ pellet (R.D. = 90%), N₂:H₂ = 1:3 gas flow for H₂ atmosphere, and 60 sccm total flow rate.

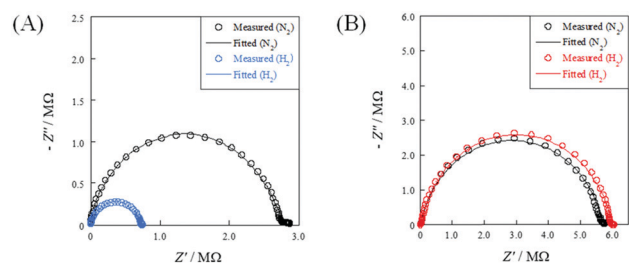
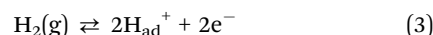


Fig. 3 Nyquist plots under N₂ and H₂ atmospheres at 723 K: (A) porous pellet (R.D. = 60%); and (B) dense pellet (R.D. = 90%).

To evaluate the relative density dependence of electrochemical conductivity, EIS measurements were conducted under N₂ or N₂ + H₂ atmospheres using porous (R.D. = 60%) and dense (R.D. = 90%) SrZrO₃ samples. Fig. 2 depicts the temperature dependence of electrochemical conductivity on each sample. Fig. 3 presents the Nyquist plot for each sample under N₂ and N₂ + H₂ atmospheres at 723 K. Accordingly, the porous sample and dense sample exhibited completely different trends. Regarding the result of the porous sample (Fig. 2(A)), the electrochemical conductivity of both the bulk and grain boundary under a N₂ atmosphere decreased along with decreasing temperature, exhibiting typical Arrhenius behavior. The apparent activation energies of electrochemical conductivity were calculated as 0.93 eV and 0.89 eV, respectively, for the bulk and grain boundary. When H₂ was supplied, the apparent activation energy of the electrochemical conductivity decreased markedly compared to that under N₂ atmosphere: 0.47 eV (bulk) and 0.74 eV (grain boundary). Regarding the dense sample (Fig. 2(B)), however, the temperature dependence and the apparent activation energy for the dense sample under a H₂ atmosphere were identical to those under a N₂ atmosphere. Such a difference between porous and dense samples might be attributable to the dissociative adsorption of the supplied H₂ on the grain surface, as described in eqn (3).



Additionally, hydrogen partial pressure (P_{H_2}) dependence was studied at 723 K with a porous sample to elucidate the surface proton contribution to the total conductivity under a H₂ atmosphere. Before varying the partial pressure, the sample was



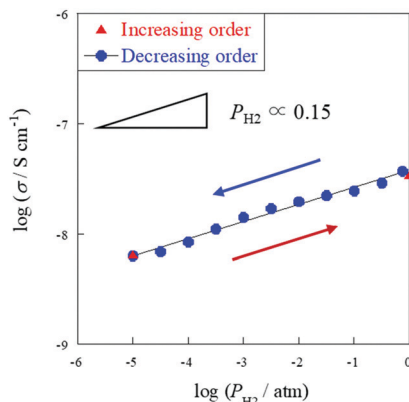


Fig. 4 H_2 partial pressure dependence of electrical conductivity on the porous $SrZrO_3$ sample (R.D. = 60%) at 723 K, $P_{H_2} = 10^{-5}$ –1 atm (N_2 balanced); total flow rate: 60 sccm.

pretreated at 723 K for 2 h under a H_2 atmosphere to mitigate changes in conductivity caused by H_2 reduction. Then H_2 partial pressure was decreased to $P_{H_2} = 10^{-5}$ atm. Impedance measurement was carried out for two plots ($P_{H_2} = 10^{-5}$ and 1 atm) with increasing order, then the measurement was continuously performed at $P_{H_2} = 10^{-5}$ –1 atm with decreasing order. Consequently, as shown in Fig. 4, positive dependence of H_2 partial pressure on the electrochemical conductivity was confirmed. Therefore, the dominant conductive carrier was inferred as electrons under a N_2 atmosphere and surface protons under a H_2 atmosphere for a porous sample, and as electrons under a N_2 or H_2 atmosphere for a dense sample. In addition, the former plot (red) and the latter plot (blue) at $P_{H_2} = 10^{-5}$ atm were exactly identical, indicating that the conductivity could be reproduced after removing surface protons. This result demonstrates that the coverage of surface OH^- groups is reversible with varying hydrogen partial pressure. The results of these investigations clarified that the decrease in apparent activation energy and the increase of conductivity under a H_2 atmosphere were attributed to H_2 dissociative adsorption on the grain surface, caused by the appearance of surface protonics.

To ascertain whether the dominant conductive carrier on the porous sample under H_2 conditions is protons or not, H/D isotope effects were assessed with the porous and dense samples. As presented in Table 1, the porous sample exhibited an H/D isotope effect at all measured temperatures ($\sigma_{D_2}/\sigma_{H_2} \approx 0.5$), indicating protons as the dominant conductive carrier. Such a significant H/D isotopic value is explainable by a semi-classical theory.^{28–33} Considering a potential barrier for proton

(or deuteron) transfer reaction, a proton's binding energy is $(1/2)h\nu_H$ at the zero-point vibration energy level. The difference in activation energy between a proton and deuteron can be shown as presented in eqn (4).

$$E_D - E_H = (1/2)h(\nu_D - \nu_H) \quad (4)$$

Assuming that the wave number is derived from the OH^- stretching frequency, correlation can be found such as $\nu \propto m^{-1/2}$, where m represents the mass of a proton or deuteron. Regarding OH^- ions in $SrZrO_3$ -based oxides, the OH^- stretching frequency is reported as around 10^{14} s^{-1} order.^{34,35} Using this value, the difference of the activation energies ($E_D - E_H$) is calculated theoretically as 0.055 eV, and the experimental results were 0.03 eV. It is slightly lower than the theoretical value, probably because a small difference in energy level exists not only at the initial state, but also at the transition state. Considering that point, a slightly lower value would typically be obtained for the difference in the activation energies.^{30,31,36} Protons are formed by H_2 dissociative adsorption on the porous $SrZrO_3$ surface. The resulting surface proton hopping dominates conduction under a H_2 atmosphere.

As mentioned above, it is indubitable that the increase of conductivity with H_2 addition is attributed to surface proton conduction. It is also important to assess the change of oxidation state by H_2 reduction. Therefore, XPS measurements were performed with $SrZrO_3$ samples which were pre-treated with various conditions: (A) N_2 purge, (B) H_2 reduction, (C) N_2 purge after H_2 reduction. Fig. 5 presents O1s XPS spectra. As a result, two peaks at around 529 eV and 531 eV were observed for all patterns ((A)–(C)). These peaks are assigned to O_s or OH and O_{lat} , respectively.^{37–40} These two peaks did not shift through (A)–(C), which indicated that the oxidation state of $SrZrO_3$ would not change even if the sample was reduced with H_2 . Furthermore, the peak intensity of O_s or OH increased after the sample was treated with H_2 ((A) \rightarrow (B)), then decreased with N_2 purge ((B) \rightarrow (C)). This indicated that surface adsorbed species *i.e.* OH groups were formed over the $SrZrO_3$ surface by H_2 reduction, and it would be removed by N_2 purge. This behavior well corresponds to the reversibility of surface OH coverage (Fig. 4).

In conclusion, through several studies of EIS measurement, surface protons under a H_2 atmosphere were investigated by examination of the relative density dependence of a $SrZrO_3$ pellet. The cause of the decrease of apparent activation energy in a porous sample by H_2 addition was inferred as proton

Table 1 H/D isotope effect values of porous (R.D. = 60%) and dense (R.D. = 90%) $SrZrO_3$ samples under $H_2(D_2)$ atmosphere: $N_2 : H_2(D_2) = 1 : 3$ gas flow, 423–723 K temperature, 60 sccm total flow rate

Temperature/K	Porous $SrZrO_3$ sample			Dense $SrZrO_3$ sample		
	$\sigma_{H_2}/S \text{ cm}^{-1}$	$\sigma_{D_2}/S \text{ cm}^{-1}$	$\sigma_{D_2}/\sigma_{H_2}/-$	$\sigma_{H_2}/S \text{ cm}^{-1}$	$\sigma_{D_2}/S \text{ cm}^{-1}$	$\sigma_{D_2}/\sigma_{H_2}/-$
723	1.21×10^{-7}	7.91×10^{-8}	0.65	2.43×10^{-6}	2.41×10^{-6}	0.99
623	1.70×10^{-8}	9.88×10^{-9}	0.58	4.14×10^{-7}	4.12×10^{-7}	1.00
523	5.01×10^{-10}	2.62×10^{-10}	0.52	2.57×10^{-8}	2.55×10^{-8}	0.99
423	4.74×10^{-11}	2.27×10^{-11}	0.48	2.44×10^{-10}	2.42×10^{-10}	0.99



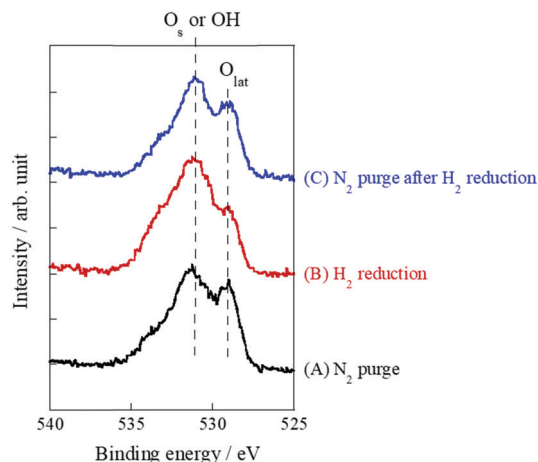


Fig. 5 O 1s X-ray photoelectron spectra of various pretreatment conditions over SrZrO₃: (A) N₂ purge, (B) H₂ reduction, and (C) N₂ purge after H₂ reduction.

formation by H₂ dissociative adsorption on the grain surface. Then proton conduction occurs under a H₂ atmosphere. H/D isotope effects indicated proton migration on the oxide surface with the hopping mechanism. Such identification of a dominant conductive carrier is an important consideration when assessing correlation between surface ion conduction and chemical reactions.

This work was supported by JST CREST JPMJCR1423.

Conflicts of interest

There are no conflicts to declare.

Notes and references

- R. Sato, S. Ohkuma, Y. Shibuta, F. Shimojo and S. Yamaguchi, *J. Phys. Chem. C*, 2015, **119**, 28925.
- M. F. Camellone, F. N. Ribeiro, L. Szabová, Y. Tateyama and S. Fabris, *J. Am. Chem. Soc.*, 2016, **138**, 11560.
- G. Tocci and A. Michaelides, *J. Phys. Chem. Lett.*, 2014, **5**, 474.
- S. Miyoshi, Y. Akao, N. Kuwata, J. Kawamura, Y. Oyama, T. Yagi and S. Yamaguchi, *Chem. Mater.*, 2014, **26**, 5194.
- S. Ø. Stub, E. Vøllestad and T. Norby, *J. Phys. Chem. C*, 2017, **121**, 12817.
- S. Kim, H. J. Avila-Paredes, S. Wang, C. T. Chen, R. A. De Souza, M. Martin and Z. A. Munir, *Phys. Chem. Chem. Phys.*, 2009, **11**, 3035.
- S. Okada, R. Manabe, R. Inagaki, S. Okada and Y. Sekine, *Catal. Today*, 2018, **307**, 272.
- R. Manabe, S. Okada, R. Inagaki, K. Oshima, S. Ogo and Y. Sekine, *Sci. Rep.*, 2016, **6**, 38007.
- S. Ogo and Y. Sekine, *Chem. Rec.*, 2017, **17**(8), 726.
- R. Inagaki, R. Manabe, Y. Hisai, Y. Kamite, T. Yabe, S. Ogo and Y. Sekine, *Int. J. Hydrogen Energy*, 2018, **43**, 14310.
- M. Torimoto, K. Murakami and Y. Sekine, *Bull. Chem. Soc. Jpn.*, 2019, **92**(10), 1785.
- R. Manabe, H. Nakatsubo, A. Gondo, K. Murakami, S. Ogo, H. Tsuneki, M. Ikeda, A. Ishikawa, H. Nakai and Y. Sekine, *Chem. Sci.*, 2017, **8**, 5434.
- A. Gondo, R. Manabe, R. Sakai, K. Murakami, T. Yabe, S. Ogo, M. Ikeda, H. Tsuneki and Y. Sekine, *Catal. Lett.*, 2018, **148**, 1929.
- K. Murakami, R. Manabe, H. Nakatsubo, T. Yabe, S. Ogo and Y. Sekine, *Catal. Today*, 2018, **307**, 272.
- K. Murakami, Y. Tanaka, R. Sakai, K. Toko, K. Ito, A. Ishikawa, T. Higo, T. Yabe, S. Ogo, M. Ikeda, H. Tsuneki, H. Nakai and Y. Sekine, *Catal. Today*, DOI: 10.1016/j.cattod.2018.10.055.
- K. Murakami, Y. Tanaka, S. Hayashi, R. Sakai, Y. Hisai, Y. Mizutani, A. Ishikawa, T. Higo, S. Ogo, J. G. Seo, H. Tsuneki, H. Nakai and Y. Sekine, *J. Chem. Phys.*, 2019, **151**, 064708.
- K. Takise, A. Sato, K. Murakami, S. Ogo, J. G. Seo, K. Imagawa, S. Kado and Y. Sekine, *RSC Adv.*, 2019, **9**, 5918.
- K. Takise, A. Sato, S. Ogo, J. G. Seo, K. Imagawa, S. Kado and Y. Sekine, *RSC Adv.*, 2019, **9**, 27743.
- M. Kosaka, T. Higo, S. Ogo, J. G. Seo, K. Imagawa, S. Kado and Y. Sekine, *Int. J. Hydrogen Energy*, 2020, **45**(1), 738.
- R. Manabe, S. Ø. Stub, T. Norby and Y. Sekine, *Solid State Commun.*, 2018, **270**, 45.
- B. Scherrer, M. V. F. Schlupp, D. Stender, J. Martynczuk, J. G. Grolig, H. Ma, P. Kocher, T. Lippert, M. Prestat and L. J. Gauckler, *Adv. Funct. Mater.*, 2013, **23**, 1957.
- S. Ø. Stub, K. Thorshaug, P. M. Røvik, T. Norby and E. Vøllestad, *Phys. Chem. Chem. Phys.*, 2018, **20**, 15653.
- S. Ø. Stub, E. Vøllestad and T. Norby, *J. Mater. Chem. A*, 2018, **6**, 8265.
- I. G. Tredici, F. Maglia, C. Ferrara, P. Mustarelli and U. Anselmi-Tamburini, *Adv. Funct. Mater.*, 2014, **24**, 5137.
- S. Raz, K. Sasaki, J. Maier and I. Riess, *Solid State Ionics*, 2001, **143**, 181.
- A. Sato, S. Ogo, Y. Takeno, K. Takise, J. G. Seo and Y. Sekine, *ACS Omega*, 2019, **4**, 10438.
- T. Higo, K. Ueno, Y. Omori, H. Tsuchiya, S. Ogo, S. Hirose, H. Mikami and Y. Sekine, *RSC Adv.*, 2019, **9**, 22721.
- A. S. Nowick and A. V. Vaysley, *Solid State Ionics*, 1997, **97**, 17.
- R. Mukundan, E. L. Brosha, S. A. Birdsell, A. L. Costello, F. H. Garzon and R. S. Williams, *J. Electrochem. Soc.*, 1999, **146**, 2184.
- T. Scherban and A. S. Nowick, *Solid State Ionics*, 1989, **35**, 189.
- T. Scherban, W.-K. Lee and A. S. Nowick, *Solid State Ionics*, 1988, **28–30**, 585.
- W.-K. Lee, A. S. Nowick and L. A. Boatner, *Solid State Ionics*, 1986, **18–19**, 989.
- T. Scherban and A. S. Nowick, *Solid State Ionics*, 1992, **53–56**, 1004.
- S. Shin, H. H. Huang, M. Ishigame and H. Iwahara, *Solid State Ionics*, 1990, **40–41**, 910.
- H. Yugami, Y. Shibayama, S. Matsuo, M. Ishigame and S. Shin, *Solid State Ionics*, 1996, **85**, 319.
- T. Norby, M. Friesel and B. E. Mellander, *Solid State Ionics*, 1995, **77**, 105.
- J. T. Newberg, D. E. Starr, S. Yamamoto, S. Kaya, T. Kendelewicz, E. R. Mysak, S. Porsgaard, M. B. Salmeron, G. E. Brown Jr., A. Nilsson and H. Bluhm, *Surf. Sci.*, 2011, **605**, 89.
- G. P. López, D. G. Castner and B. D. Ratner, *Surf. Interface Anal.*, 1991, **17**, 267.
- E. McCafferty and J. P. Wightman, *Surf. Interface Anal.*, 1998, **26**, 549.
- J. van den Brand, W. G. Sloof, H. Terryn and J. H. W. de Wit, *Surf. Interface Anal.*, 2004, **36**, 81.

